INTRODUCTION

Geothermometers are natural mineral systems that may be used to estimate the temperatures that produce an equilibrated mineral assemblage in a metamorphic rock through element partitioning between minerals. Element partitioning between mineral phases is a chemical reaction, independent of volatiles, and is useful for establishing peak metamorphic temperatures (Ferry and Spear, 1978). Garnet-biotite geothermometers are a mathematical attempt to correlate temperature and the elemental partitioning of Mg and Fe^{2+} between coexisting garnet and biotite crystals. The garnet-biotite thermometer is particularly useful because of the common occurrence of garnet and biotite together in medium metamorphic grades and in rocks of different bulk compositions. This relationship is significantly dependent on temperature, and is generally calculated with little focus on the effects of pressure. However, pressure may affect change equilibria. Most current garnet-biotite geothermometers are calibrated at low pressures around 2kbars; this study is calibrated at 8kbars of pressure. With the wide range of coexisting garnet-biotite metamorphic occurrences, creating an accurate geothermometer calibrated under comparable metamorphic pressures would have a wide range of applications in metamorphic petrology.

Since Perchuk (1967), there have been twenty-one different formulations of the garnet-biotite geothermometer (Wu and Pan, 1999) including Ferry and Spear, (1978). Only three of these geothermometers are experimental calibrations, while the remaining eighteen are empirical calibrations. This large number of garnet-biotite geothermometers reflects the conflicts and complexity of creating an accurate geothermometer. The concept of a geothermometer does not account for the multi-dimensionality of metamorphic conditions, especially considering that metamorphism is a function of both temperature and pressure. These existing geothermometers

give widely varying temperature estimates for the same rock. Two of the three experimental calibrations did not investigate pressures outside of the 2kbar range, and the third only conducted experiments with pressures at 6kbars. Without a pressure that accurately reflects common metamorphic conditions, these geothermometers are only a partial representation of the chemical reaction that takes place in nature.

This study is an experimental calibration of a garnet-biotite geothermometer using experimental methods based largely on Ferry and Spear's (1978) widely cited experimental calibration of a garnet-biotite geothermometer. However, this study will use natural garnets and biotites instead of synthetic materials like Ferry and Spear (1978) because they represent the most realistic circumstances and utilizations of a garnet-biotite geothermometer. In keeping with Ferry and Spear's (1978) methods, the garnet and biotite are ground together in a mixture with a molar ratio of 98/2 to limit the change needed in garnet during reaction. The use of natural minerals brings into consideration the effects of minor elements, such as Mn in garnet and Ti in biotite. In addition, a pressure of 8 kbars is used to approximate the conditions of many regional metamorphic rocks.

BACKGROUND INFORMATION

Geothermometery and Equilibrium Constants

Element partitioning in the garnet-biotite geothermometer is the measured exchange of Fe^{2+} and Mg^{2+} ions with temperature and pressure changes. The exchange reaction can be written as:

phlogopite + almandine = annite and pyrope,

or

$$X_{Mg}^{Bt} + X_{Fe}^{Grt} = X_{Fe}^{Bt} + X_{Mg}^{Grt}.$$

To quantify this relationship, an equilibrium constant is calculated to relate the ratios of Mg and Fe in garnet and biotite at a specific temperature and pressure. For the garnet-biotite geothermometer, the equilibrium constant is primarily a function of temperature. The equilibrium constant is written as:

$$K_D = \frac{X_{Fe}^{Bt} \cdot X_{Mg}^{Grt}}{X_{Mg}^{Bt} \cdot X_{Fe}^{Grt}} \quad \left(= \frac{\text{component proportions on right - hand side}}{\text{component proportions on left - hand side}} \right)$$

Garnet

Group	End Member	Composition	*n*		G(calc)
			Pure Synthetic	**Normal Range**	
Pyralspite	Pyrope	$Mg_3Al_2(SiO_4)_3$	1.714	1.720-1.770	3.582
	Almandine	$Fe_3Al_2(SiO_4)_3$	1.830	1.720-1.820	4.315
	Spessartine	$Mn_3Al_2(SiO_4)_3$	1.800	1.790-1.810	4.197
Grandite	Grossular	$Ca_3Al_2(SiO_4)_3$	1.734	1.735-1.770	3.594
	Andradite	$Mg_3Fe^{3+}{}_2(SiO_4)_3$	1.877	1.850-1.890	3.859
	Hydrogrossular	$Ca_3Al_2(SiO_4)_{3-x}(OH)_{4x}$	----------	1.675-1.734	3.1-3.6

Table 1: Compositional end members and chemical properties of garnet.

Garnet has the chemical formula, $X_3Y_2(SiO_4)_3$, with two crystallographic sites, X and Y, for different cations, any combination of which produces different end-members (Table 1). Pyrope is the Mg end-member of the pyralspite group with the chemical formula $Mg_3Al_2(SiO_4)_3$. Almandine is the Fe^{2+} end-member with the formula $Fe_3Al_2(SiO_4)_3$. Garnet has an isometric crystal structure (4/*m***3**2/*m*) where isolated silicon tetrahedrons are bonded together with the other cations in 6 and 8-fold coordination. Si tetrahedrons and Y octahedrons share oxygen anions to form chains parallel to the *a* axes. The spaces between the chains are distorted 8-fold sites occupied by the X cations, Mg^{2+} and Fe^{2+}. Garnet crystals are brittle, euhedral-subhedral with no cleavage and they fracture conchoidally. They have a hardness ranging between 6-7 and a specific gravity of 3.1-4.2 (Nesse, p.310). Garnet occurs in a wide range of metamorphic grades.

Pyrope is commonly associated with ultramafic igneous rocks and at the higher temperatures associated with high grade metamorphism. Almandine is typical of medium grade metamorphic mica schists and gneisses (Nesse, p. 311).

Garnet's flexible crystal structure can change its size to accommodate variously sized cations, such as Mn^{2+} and Ca^{2+} as well as Mg^{2+} and Fe^{2+}. The substitution of larger Ca^{2+} and Mn^{2+} ions for Mg^{2+} and Fe^{2+} produces localized structural expansions. As a result, Fe^{2+} is preferentially incorporated in the garnet crystallographic structure to increase overall unit cell size and to minimize local inter-crystalline strain (Dallmeyer, 1974). Despite this accommodating crystallographic structure, garnet it slow to react in element partitioning (Ferry and Spear, 1978). Garnet crystals tend to be zoned; therefore the rims are the most reactive. As a result, the cores of garnet crystals remain largely unaltered due to their sluggish reaction. This reactive property can have adverse effects on garnet-biotite geothermometers if crystals are too large in the experiment. Changes in K_D values between garnet rims and biotite with metamorphic grade provide further evidence for reactive garnet rims (Osberg, 1971).

Biotite

End Member	Composition	Additional Properties
Annite	$KFe_3AlSi_3O_{10}(OH)_2$	G = 2.7-3.3
Phlogopite	$KMg_3AlSi_3O_{10}(OH)_2$	n_α = 1.522-1.625
Siderophyllite	$KFe_2Al(Al_2Si_2O_{10})(OH)_2$	n_β = 1.522-1.625
Eastonite	$KMg_2Al(Al_2Si_2O_{10})(OH)_2$	n_γ = 1.522-1.625

Table 2: Compositional variations and properties of biotite.

Biotite has the chemical formula, $KX_3AlY_3O_{10}(OH)_{12}$. The X and Y sites can be occupied by a variety of cations, producing a variety of end members (Figure 1). The two end-members relevant to this study are annite ($KFe_3AlSi_3O_{10}(OH)_{12}$) and phlogopite ($KMg_3AlSi_3O_{10}(OH)_{12}$).

The X site typically substitutes Mg^{2+} and Fe^{2+} while the Y crystallographic site substitutes either Si or Al.

Biotite is a common mineral, present in igneous, sedimentary and metamorphic rocks. In metamorphic rocks, biotite occurs in hornfels, phyllites, schists, and gneisses (Nesse, p. 248). Biotite has a hardness of 2-3 and specific gravity of 2.7-3.3. Crystals occur in hexagonal, collumnal "books" of crystals, where perfect {001} cleavage produces thin elastic foils. Biotite has a monoclinic crystal structure (2/*m*) for the common 1*M* polytype, whose unit cell is one TOT+ *c* layer thick. A TOT layer is comprised of two tetrahedral layers sandwiching an octahedral layer between them. These TOT layers are held together by a weak monovalent (typically K^{+}) ionic bond, because the TOT layers have a net negative charge. In crystals with compositional irregularities, the octahedral substitution of Ti, Al and Fe^{3+} increases the positive charge on the biotite octahedral layer. In order to accommodate excess positive charges, biotite increases tetrahedral substitution of Al for Si to provide less positive charge on the tetrahedral layer and using unoccupied octahedral positions to produce negative charges in the octahedral layer (Dallmeyer, 1974).

The primary substitution affecting the tetrahedral layer results from substituting Al for Si, thereby enlarging the tetrahedral layer in the TOT structure. In contrast, the octahedral sites may substitute Ti, Al and Fe^{3+} for Fe^{2+} and Mg when there is an increase in the number of vacant octahedral positions reducing the dimensions of the octahedral layer. Typically, the slightly larger Fe^{2+} is preferred over Mg in the biotite octahedral layer in order to stabilize the structural deformation. Substitutions of different cations have various effects on the $K_D^{Bi\text{-}Gar}$. Under similar conditions, increasing the dimensions of the octahedral layer with substituting Ti, Al, and Fe^{3+} would also raise the value of $K_D^{Bi\text{-}Gar}$. Titanium has two additional positive charges whereas

aluminum and ferric iron only carry one. As a result, there is a positive correlation of $K_D^{Bi\text{-}Gar}$ with increased octahedral substitution of Ti, Al and Fe^{3+}, where Ti exerting the most control on the effects on $K_D^{Bi\text{-}Gar}$ (Dallmeyer, 1974).

Previous Research

There are several inherent problems with the garnet-biotite geothermometer. Firstly, many versions of the geothermometer assume ideal Fe-Mg mixing; the non-ideal properties of both garnet and biotite are not considered completely since the minor elements are almost neglected. Using synthetic materials and assuming ideal Fe-Mg mixing eliminates the consideration of naturally occurring impurities and their effects on the chemical reaction and the exchange of Fe^{2+} and Mg^{2+} ions. Without the consideration of minor elements, the resultant geothermometer may reflect a more precise relationship of pure Fe-Mg mixing. However, the geothermometer will not be as useful when considering natural materials. Secondly, the effects of pressure on equilibrium are not typically considered in existing geothermometer calibrations (Wu and Pan, 1999). The first problem is mainly addressed by using a non-ideal solid solution, because it can account for the compositional irregularities of natural specimens. Problems do arise from using either synthetic or natural specimens. Synthetic specimens represent highly unlikely occurrences in nature, but the natural specimens incorporate compositional irregularities that require special consideration.

There are two methods to calibrate a geothermometer, empirical calibration through statistical regression, as demonstrated by Dasgupta et al. (1991) and experimental calibration as calculated by Ferry and Spear (1978) and Perchuk et al. (1984). A significant paper (Ferry and Spear, 1978), studied the Mg and Fe^{2+} cation exchange described by the reaction $Fe_3Al_2Si_3O_{12} + KMg_3AlSi_3O_{10}(OH)_2 = Mg_3Al_2Si_3O_{12} + KFe_3AlSi_3O_{10}(OH)_2$ using synthetic garnet ($alm_{80}py_{20}$ and

$alm_{90}py_{10}$) and synthetic biotite ($ann_{25}phl_{75}$, $ann_{50}phl_{50}$, $ann_{75}phl_{25}$, $ann_{100}phl_{0}$). The synthetic reactants were >99% biotite or garnet, thus reducing the compositional margin of error in this experiment. However, the Fe^{3+} content of the synthesized biotite is estimated to be around 7% (Holdaway et al., 1997).

Ferry and Spear (1978) chose to use a garnet-biotite molar ratio of 98/2 in their partitioning experiment. This molar ratio was advantageous because the bulk composition of the garnet is slow to react in this chemical equation, did not have to change significantly in order to reach equilibrium. Ferry and Spear used mass-balance corrections for small changes in garnet composition that resulted from shifts in average biotite composition (Holdaway et al., 1997). The experimental study was conducted at a constant pressure of 2.07kbars, and tested a range of temperatures between 550 and 800°C. The model created by Ferry and Spear has been applied to other studies (eg. McClellan, 2004) and has been further expanded by Kleeman and Reinhardt (1994) to utilize non-ideal partitioning and accommodate compositional irregularities, such as Ca^{2+} and Mg^{2+} substitution for Fe^{2+} and Mg^{2+} in garnet.

Experimental data sets are the building blocks of empirical calibrations. Holdaway et al. (1997) used data sets, assumptions and Margules parameters from Ferry and Spear (1978), Perchuk and Lavent'eva (1983) Mukhopadhyay et al. (1997) and Ganguly and Cheng (1994). Margules parameters are values calculated for minerals to correct for compositional variations and irregularities. They follow a theoretical model of the effect of compositional changes in a mineral's free energy and the effects on their equilibrium with other minerals. More specifically, Holdaway et al., (1997) adopted Mukhopadhyay et al. (1997) Margules parameters for Fe-Mg-Ca interactions in garnet including a ternary W_{FeMgCa} parameter where (T is temperature in K):

W_{MnCa} = 1425 J/mol (Ganguly and Cheng 1994)
W_{MnFe} = 1860 J/mol (Pownceby et al., 1987, Ganguly and Cheng 1994)

W_{MnMg}= 30345-15.6T J/mol

The Margules parameters for biotite are treated differently that those for garnet. Determining bioite Margules parameters is an iterative stepwise linear regression. Two steps were applied to Perchuk and Lavent'eva's (1983) temperature calculations using their chemical and experimental data. No parameter was calculated for Fe^{3+} content. The formula for the biotite Margules parameters is (again T is temperature in K):

ΔW_{Ti} = 310,990-370.39T J/mol

Ferry and Spear (1987) used mass-balance corrections for small changes in garnet composition that resulted from shifts in average biotite composition, but that could not be detected by their microprobe. This analysis was not applied to Al and Si in their biotite samples, and assumed to be zero. Analyses were made using a 2 to 98 garnet to biotite ratio. Without correcting for Al^{Bt}, any version of Ferry and Spear's calibration applied to the Perchuk and Lavent'eva chemical data gives higher temperature estimates than experimental temperature estimates, being above 600°C. The Perchuk and Lavent'eva (1983) data is considered important for determining the Fe-Mg Margules parameters in biotite including temperature dependence, but less so in determining the Al Margules parameters. However, this data set was of no value in determining or testing the garnet Mn or Ca interactions and biotite Ti interactions. (Holdaway et al., 1997). Empirical calibrations through regression analysis use only a small amount of data that is not necessarily consistent in its applications as data may be extracted from both natural pairs and literature (Wu and Pan, 1999). This would bring about an inconsistent data set, because the different parameters of individual data sets may create problems with new calibrations. As a result, the accuracy and precision of the produced data will be of different magnitudes.

Existing formulations of garnet-biotite thermometer are inadequate to estimate temperatures in rocks of widely varying bulk compositions, although each may work well within limited compositional ranges (Dasgupta et al., 1991). The garnet-biotite geothermometer cannot be treated as a simple binary solution (ideal solid-solution) because of the octahedral substitution of Ca and Mn in garnet and Ti, Al and Fe^{3+} in biotite. They create charge anomalies in the crystal structure that results in preferential distribution of Fe^{2+} in comparison to Mg (Dallmeyer, 1974). However, there have been successes with a pure ln K_D thermometer, but any new formulation must incorporate the excess free energy of non-ideal mixing in garnet and biotite solid solution (Dasgupta et al., 1991).

Wu and Pan (1999) conclude that more experimental calibrations are needed to better understand this chemical relationship since empirical calibration of the partitioning of Fe^{2+} and Mg focuses on the compositions of biotite and garnet crystals from natural specimens for which the temperature of crystallization was estimated by independent means.

METHODS

Preparation Materials

Natural garnet and biotite crystals for the experiments were extracted from source rocks using pliers and tweezers, 0.3161g, and 0.6604g for the Fe- and Mg-richer garnets, and 1.0325g and 0.9087g, respectively, for the Fe- and Mg-richer biotites. After grinding the materials with a corundum mortar and pestle to have individual grains with a radius of 1-5 μm, the grain size was checked using a petrographic microscope. No further preparation was necessary for the biotite samples once they were extracted and ground.

A sample assembly (Figure 1) was then prepared by fitting and gluing a graphite tube and base disc inside a pyrex glass tube. Two types of MgO were used as filling components within

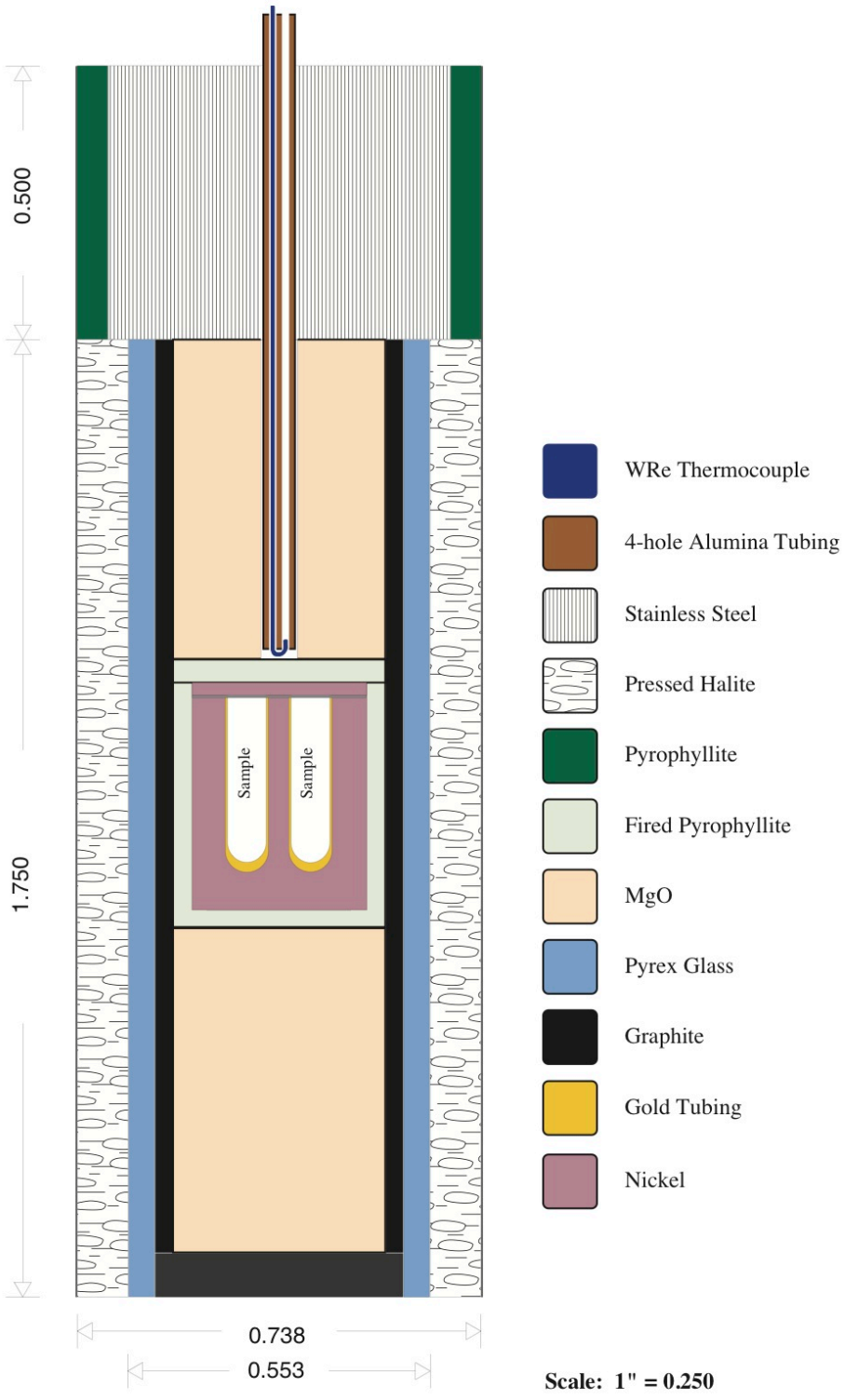

Figure 1: Materials of the sample assembly as prepared for the piston cylinder press.

the graphite tube. The upper piece of MgO was bored through the middle to allow for the alumina tubing of the thermocouple assembly and was cut with a jewelry saw to a length of 13.75mm. The lower piece of MgO was 15.75mm in length and solid through the middle. Around the pyrex glass tube was a constructed salt sleeve made by compressing powdered table salt (NaCl) inside a mold with a hand-pumped hydraulic press applying up to 15 tons of force. Two salt sleeves approximately 22mm in length were used to for the salt sleeve for each sample assembly since the mold is not large enough to produce a single salt sleeve long enough for the pyrex glass tube. The sample assembly was then wrapped in a sheet of Pb foil before it went into the pressure vessel of the piston cylinder press. The base plug and base plug sleeve rested on the sample assembly. Like the upper piece of MgO, the base plug was cored to allow for the thermocouple assembly.

The thermocouple assembly was prepared by inserting two tungsten wires through two of the holes in the 2.5-3" long 4-hole alumina tubing. They were kept separate in order to prevent the wires from crossing and completing the electrical circuit prematurely. The wires used were tungsten-rhenium alloys, being 3% and 25% tungsten. At the terminal end of the thermocouple assembly (Figure 2), the wires were deliberately crossed and reinserted into the remaining two holes in the alumina tubing. The wires needed to be in contact at the terminal end or the electrical circuit

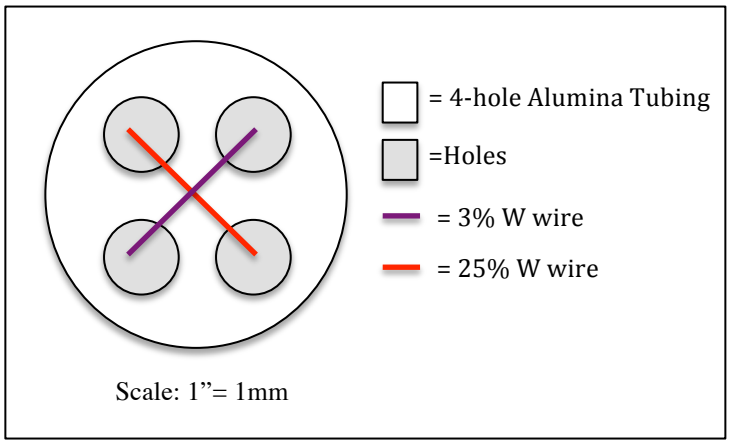

Figure 2: Cross-section of the thermocouple assembly. The thermocouple wires are crossed in an x-shape to complete the electrical circuit, creating the heat for the Fe and Mg exchange.

would not give the correct temperature of the sample. When the thermocouple assembly was inserted into the sample assembly, the terminal end was in direct contact with the pyrophyllite container around the graphite or nickel container.

Assembly of the piston cylinder press took place after the thermocouple and sample assemblies have been constructed. The piston cylinder is comprised of several parts, shown in Figure 3. The sample assembly was located within the pressure vessel. The thermocouple assembly ran through the slotted plate, the top plate and into the pressure vessel.

Garnet Homogenization and Synthesis

Short, high temperature runs were used to homogenize the chemical compositions of the pyrope and almandine. This was done to eliminate compositional zoning in the garnets that could possibly affect the Fe and Mg exchange during the experimental runs. Rather than the nickel container as shown in Figure 2, the garnet homogenizing runs used single-holed graphite containers. Garnet homogenization runs were held at a constant temperature of 1300°C and pressure of 8 kbars (approximately 2610 psi of force on a 0.75" diameter piston). We ran a total of three homogenizing runs, two for almandine-rich garnet and one for the pyrope-rich garnet. The pyrope run homogenized 0.6604g of garnet and lasted a total of 23 hours before hydraulic leaks caused the pressure to fail and quench the sample. The first homogenizing almandine run produced 0.3161g garnet and lasted 50 hours before quenching.

We attempted a second homogenizing run in order to have more almandine available for the experimental runs. The second almandine homogenization ran for 86 hours. The run melted and produced 0.3443g of almandine glass. We were not able to use this material in the experimental ion exchange runs. Therefore, we attempted to synthesize the garnets to create usable material for the experimental ion exchange reactions. The glass from the melted

Figure 3: Photograph of piston cylinder press during the 700°C run. Main components of the press are labeled in red. Parts not seen in this image are the thermocouple assembly, the carbide pusher, piston, donut and spacer. Recirculating water hoses connect the bridge and the top plate.

homogenizing run was powdered and run in the piston cylinder press for a total of 28 hours at 1100°C and 15 kbars (approximately 4984 psi). The temperature and pressure was changed from the values used for the homogenizing runs in order to promote slow garnet crystal nucleation and growth from the powdered glass.

Experimental Runs

The nickel containers were oxidized over a period of 12 hours in an oven set at 1000°C. Gold liners were fixed to the bored sample compartments in order to prevent water loss and contamination of the samples with nickel during experiment runs.

Because of garnet's sluggish reaction capacity, we used a 98/2 garnet-biotite ratio in the experimental samples. This is actually advantageous because two mixtures with very similar garnet bulk compositions (solid circles on tie lines A and B in Figure 2) and different biotite compositions held at a constant temperature and pressure will rotate the A and B tie lines to the equilibrium tie line (Z). The biotite composition in the mixtures changes considerably while the bulk composition of the garnet changes very little.

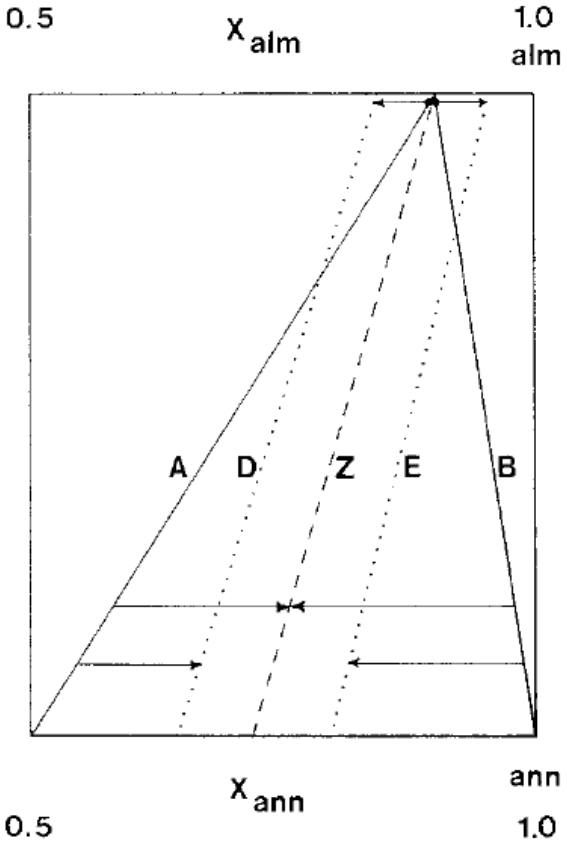

Figure 4: Compositions of coexisting biotites and garnets at some arbitrary temperature and pressure.

The garnet biotite mixture was prepared using a precision balance to measure the right proportions of materials. Two microliters of water were added in order to keep the biotite hydrated during the experimental runs. Once filled with the

98-2 mixture of garnet, biotite and water, a gold foil was placed over the top of the sample before the nickel top sealed the sample within the pyrophyllite container.

We ran a total of three experimental runs at 600°C, 700°C and 800°C, lasting 196 hours, 382 hours and 214 hours respectively. Each run maintained a pressure of 8 kbars (2610psi).

Analyses

Chemical analyses of the samples were made using the scanning electron microscope (hereafter SEM). One method of collecting data was by creating a phase diagram. This method involved mapping software that grouped similar spectra as a specific color in order to create a pixelated image of the area that described its chemistry. A second method of collecting data was to collect a spectrum of a point or small area and quantify it. This result was then entered through a series of calculations to produce a working chemical formula of the mineral under study.

Experimental Problems

There were several equipment malfunctions through the course of this study. The first homogenization run failed after twelve hours because of a hydraulic leak in the lower ram valve. Because of the resulting decrease in pressure, the thermocouple lost contact with the sample assembly and did not accurately read the temperature. In addition, the drop in pressure activated the automatic-shut down of the piston-cylinder press. The first synthesis run also failed because the thermocouple assembly lost contact with the sample assembly during the run. However, there was no hydraulic fluid leak facilitating a drop in pressure that would account for the disconnection between the thermocouple and sample assemblies.

The recirculating pump broke twice between runs, most likely due to clogging or air bubbles being introduced into the system during the disassembly of the piston cylinder. This pump serves to circulate water through the system to cool the sample during experiments.

Fortunately, there was no effect on the experiments themselves. However, it did change the procedures used during the start-up and quenching of runs.

RESULTS

Source Materials and Homogenization Runs

Figure 5 is a backscatter electron image (hereafter BEI) of the materials used in the chemical analyses of the homogenization, synthesis and experimental runs and their preparation.

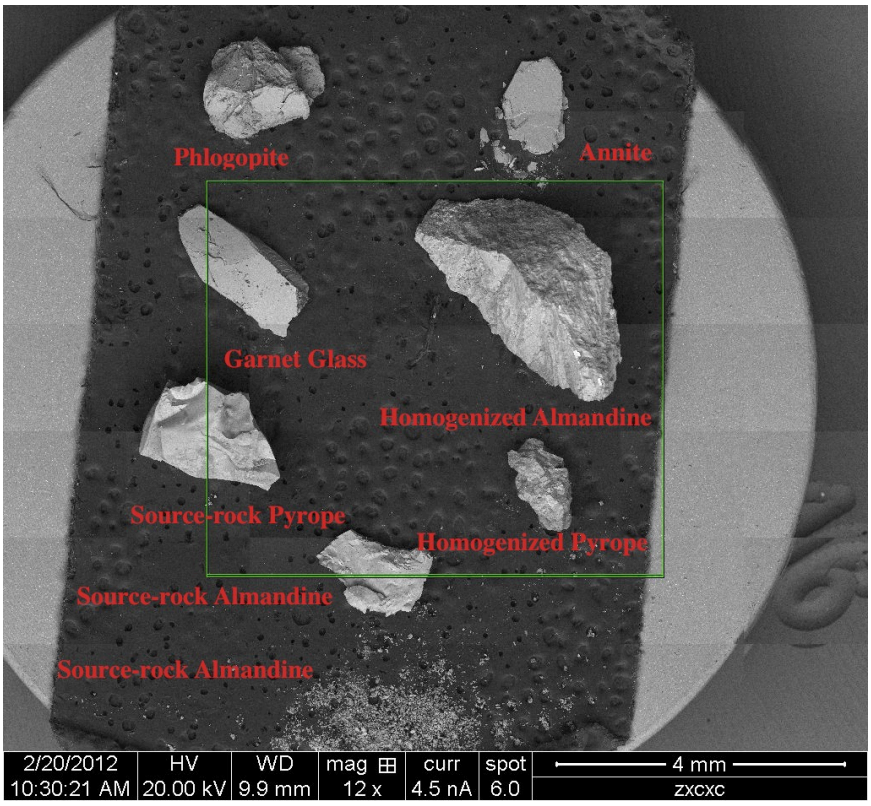

Figure 5: BEI map of specimens analyzed on the SEM. These materials were used for the analysis of the homogenized garnet and source rocks.

All chemical analyses were made on the Scanning Electron Microscope (hereafter SEM) and through a series of calculations to determine the chemical formulas of each mineral studied. All weight percentages of oxides and the calculations of resulting mineral formulas are recorded in Appendix B. The Mg number of these analyses were calculated using the formula: 100*Mg/(Fe+Mg) and are also fully reported in Appendix B. The Mg number is used to describe the ratio of Mg to Mg+Fe.

The phlogopite-rich biotite has the chemical formula $K_{0.84}Mg_{1.40}Fe_{0.75}Al_{1.41}Si_{2.54}O_{10}(OH)_2$, meaning that this biotite sample has an Mg number of 65. The second biotite has an Mg number of 38 and has the chemical formula $K_{0.87}Mg_{0.69}Fe_{1.11}Al_{1.63}Ti_{0.11}Si_{2.55}O_{10}(OH)_2$. These source materials were used directly in the experimental runs, without any modification or additional processes. The almandine-rich source garnet has an Mg number of 38. The pyrope-rich source garnet has an Mg number of 79. The homogenized pyrope has an Mg number of 45. The homogenized almandine has an Mg number of 42. The homogenized almandine contains quartz inclusions as shown in Figure 6.

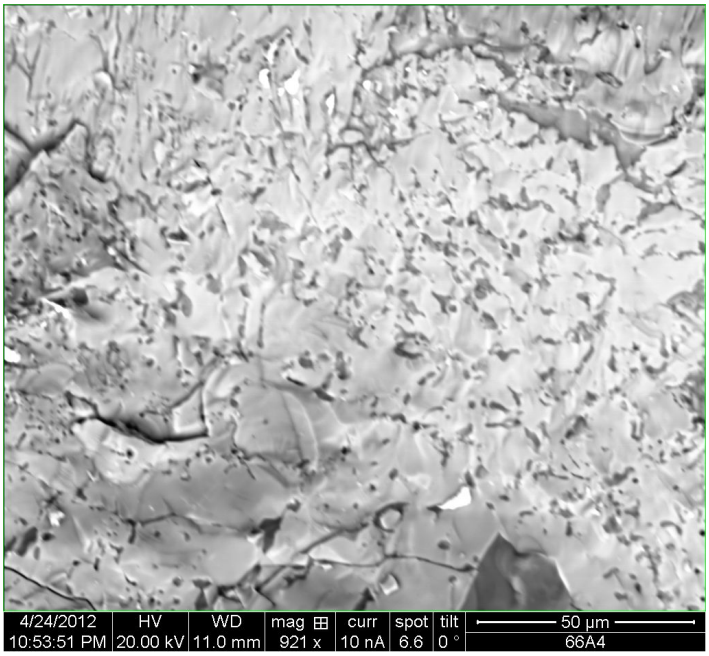

Figure 6: Quartz inclusions in the homogenized almandine

Synthesis Run

Figure 7 is a phase map of the area shown in Figure 8B. The red and purple show the location of the glass still remaining in this run while the blue and green chiefly denote the garnet crystals. The blue area is the only phase identified as containing Mg, while the green is more Fe-rich. Figure 8 is a backscattered electron image (hereafter BEI) showing the garnet glass produced by the melted synthesis run and the perfectly shaped euhedral garnet crystals that nucleated from the glassy matrix during the synthesis run. The crystals' compositions are

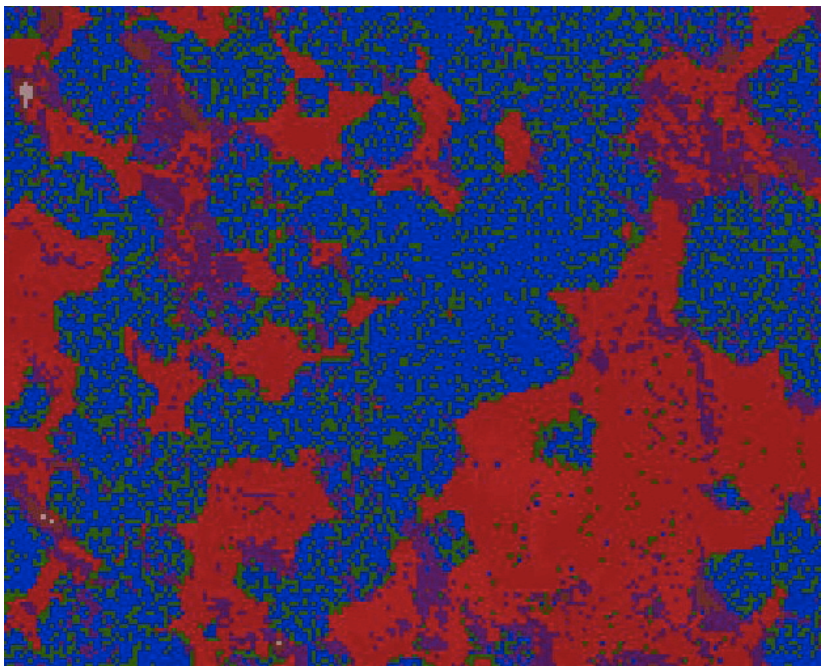

Figure 7: Phase map of the synthesis run.

consistent with almandine-rich garnet (Appendix B, column 9), though Mg is also present in the garnet.

The Mg number changed slightly during each run from the source almandine, and through both the melted homogenization and synthesis runs (Table 3). The chemical analyses of the glass from the synthesis run show a high concentration of Fe and Mg in the glassy matrix.

Source Almandine	Glass from Melted Run	Glass Remaining in Synthesis Run	Synthesized garnets
0.966 ± 0.02	0. 973 ± 0.02	0. 985 ± 0.02	0.978 ± 0.02

Table 3: Table of changing Mg/Fe ratios. These calculated values are accurate ± 0.02.

600°C

The 600°C experimental run contained spinel, quartz, garnet and an iron-rich aluminosilicate. Their characteristic straight edges and right-angle corners identified spinel crystals. Figure 9A exhibits a unique pattern of intermingled quartz and garnet; it is the only sample in this experimental run to exhibit this patterning. However, massive garnet crystals interspaced within quartz do also exist in this sample. Figure 9B and 9D exhibit a rod-like garnet growth among the massive crystals. Figure 9C shows a number of garnet crystals that are pitted

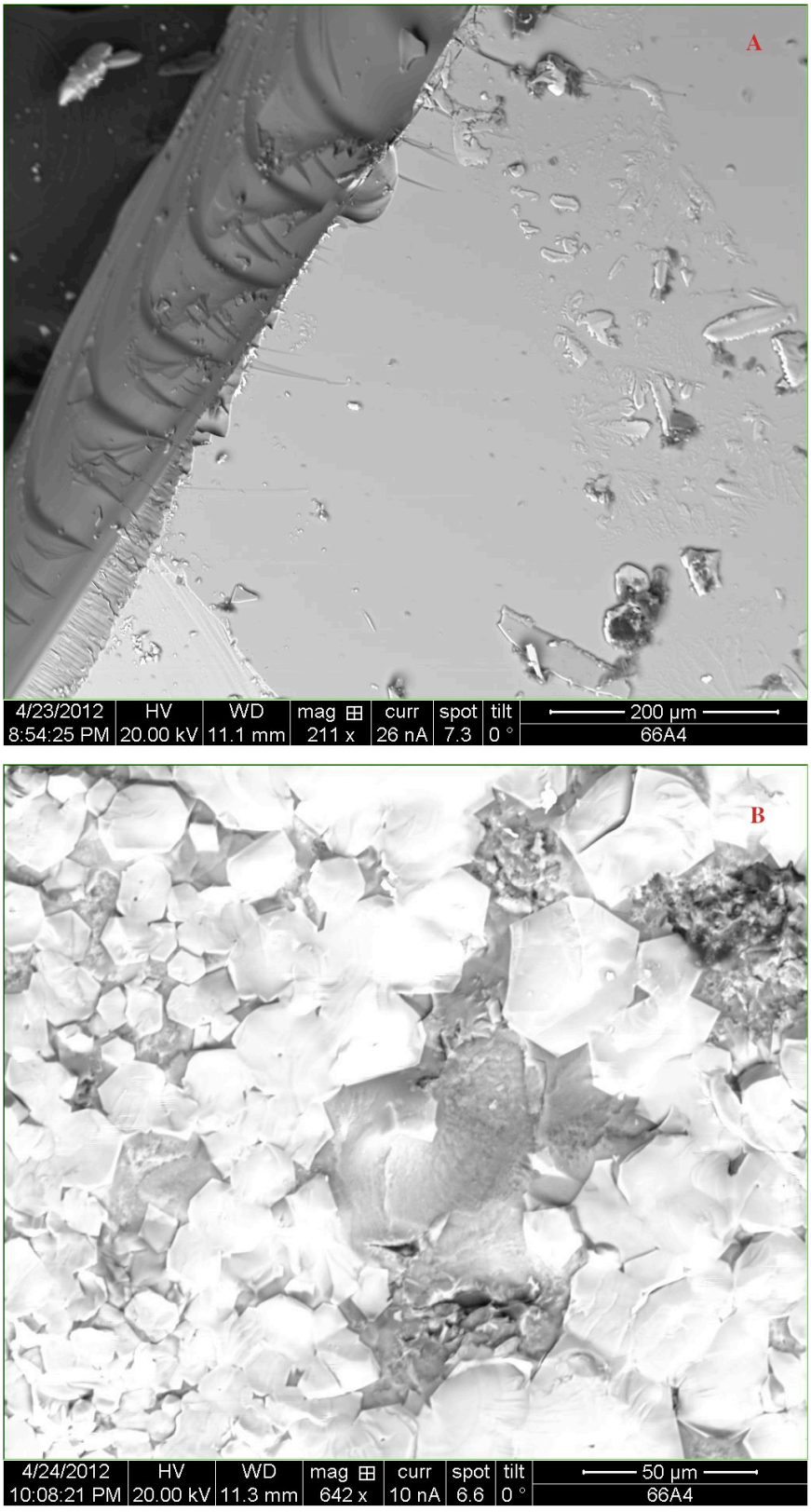

Figure 8: A) Garnet glass produced by the melted homogenization run. B) Garnet crystals nucleated from the garnet glass created by the melted homogenization run. The garnet crystals are light in this image, whereas the uncrystallized glass is gray

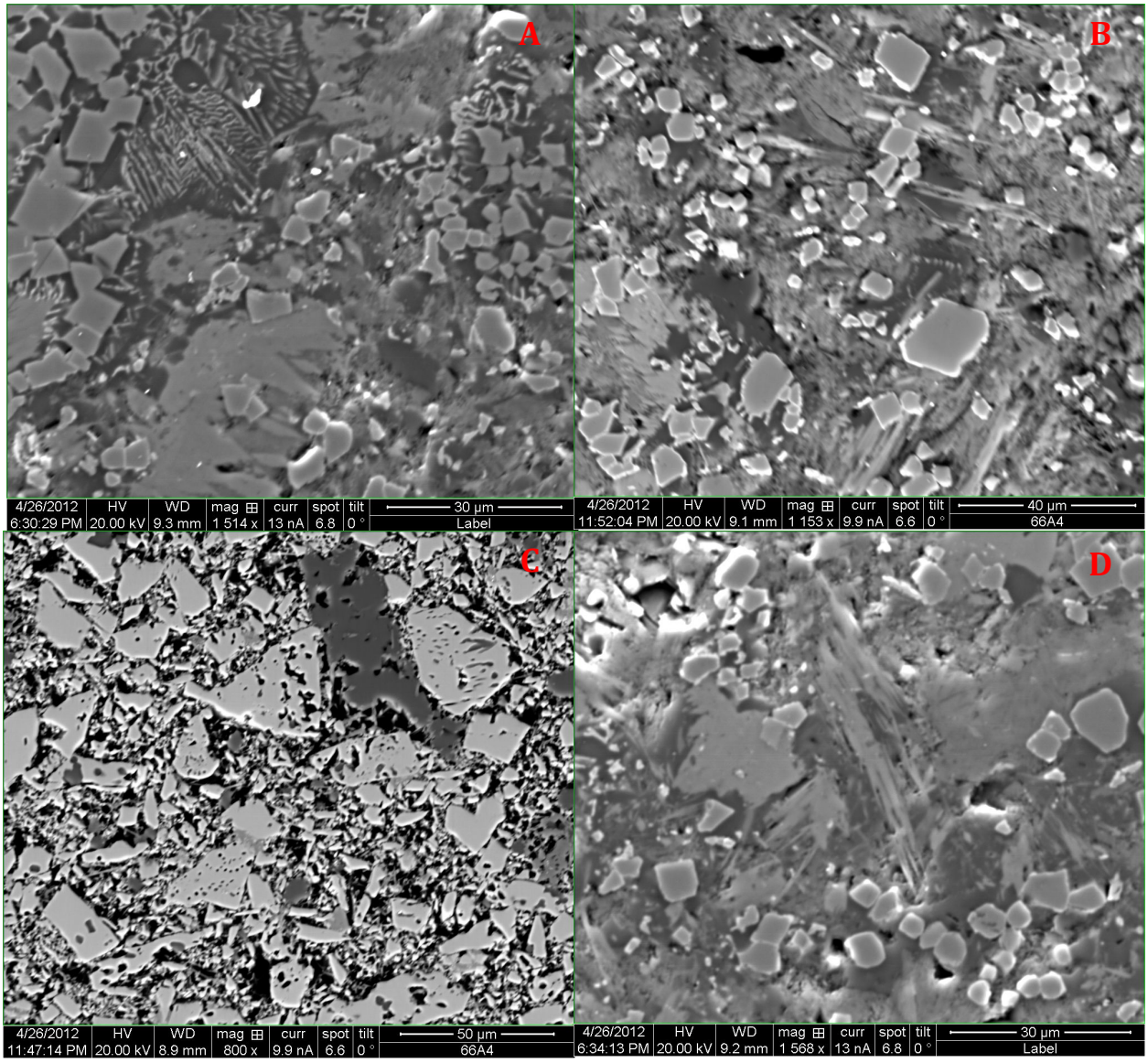

Figure 9: BEIs of each 600°C sample. A) Garnet and quartz in intermingling patterns. Spinel crystals are grouped in the upper right corner. B) Spinel crystals and rod-like garnet crystals. C) Garnet and quartz crystals exhibiting a pitted texture. D) Spinel and garnet crystals, massive and rod-shaped with quartz.

and have quartz inclusions, giving it a dotted texture. The light gray crystals are garnet and the darker, gray crystals are quartz. No biotite was identified in this field of view.

The chemical analyses of the garnet compositions of the four samples of this experimental run are listed in Appendix B.

700°C

Minerals observed in this experimental run include the same as those identified in the 600°C run. However, this sample set produced an iron oxide that could be either magnetite or hematite (Figure 10A). Blade-like crystals of kyanite were observed in this sample. Staurolite crystals were also observed in this sample, as identified by their characteristic twinning and cross-section (Figure 10B). No definitive chemical analyses were made of the staurolite crystals; they were too small to collect an adequate analysis to determine the chemical formula of the crystal. The kyanite crystals are also very small, therefore chemical analyses also contained quartz matrix. Two of the samples in the 700°C experimental run (Figure 11) produced the same texture as shown in Figure 9C.

The chemical analyses of the garnet, spinel and aluminosilicate compositions for the four samples of this run are listed in Appendix B.

800°C

These samples have a very different texture than those observed in the other experimental runs. Garnet, biotite and an iron-rich alumino silicate were the only identified minerals in these samples. The alumino-silicate crystals are the dark gray in Figure 12. Melt was observed in Figure 12A; the melt is similar to biotitic composition, but it lacked cleavage. Higher quantities of biotite were observed in this run than in the 600 and 700 degree run. There was also a high proportion of quartz in this sample.

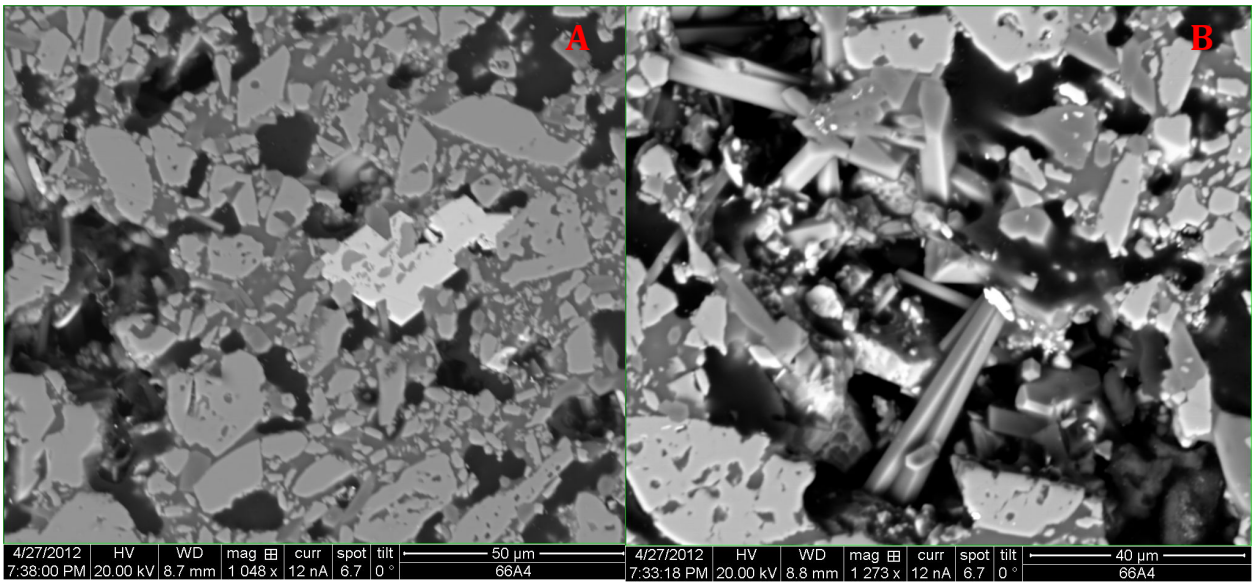

Figure 10: BEI of A) Unidentified iron-oxide mineral, garnet, quartz aluminosilicate mineral. B) Garnet, staurolite and quartz crystals from sample 2 of the 700°C experimental run. The staurolite twinning is in the upper-left corner.

DISCUSSION

The experimental ion exchange runs underwent unexpected chemical reactions and produced several new minerals including spinel, kyanite, quartz, an iron oxide and a Fe-rich alumino-silicate. The spinel was identified by its characteristic shape and chemical composition. The color difference between the rims and core in Figure 9B indicate that these crystals are zoned with a Fe-rich rim and Mg-rich core. This could result from the same properties that pertained to the synthesized garnet.

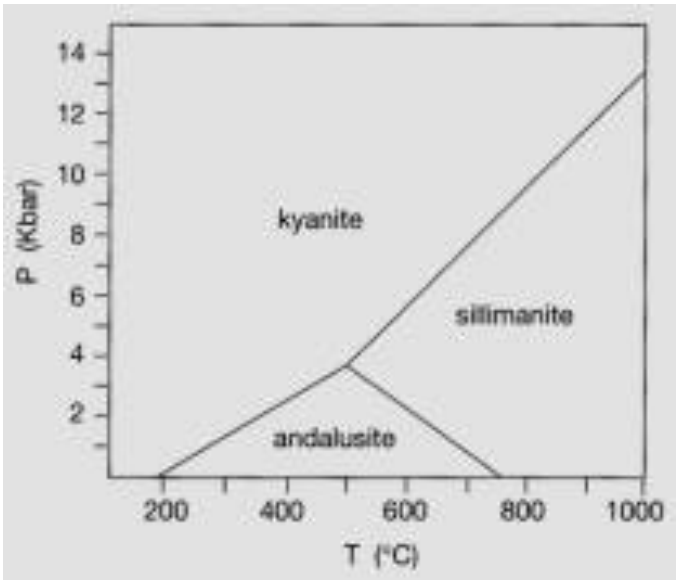

Figure 14: Aluminum oxide triple point. This is a relationship based entirely on temperature and pressure. Adapted from Cashman 2012.

The aluminum oxide observed in the samples is kyanite in the 600°C run, but becomes sillimanite in the 700°C and 800°C runs. Figure 14 defines the thermal, mineralogical relationship at the aluminum oxide triple point. The Fe-rich alumino-silicate has not yet been identified, but was chemically mapped as having relatively equal proportions of Si, Fe, Al and O. Quartz is a natural byproduct of the reaction. Therefore, its presence in every sample of each experimental run is not surprising. The garnets have quartz inclusions, producing the unusual patterns seen in Figure 8 and Figure 10.

The iron oxide mineral in Figure 10A may be magnetite or hematite. The parallelogram shape of the mineral indicates that it is hematite. However, the system was closed with little free oxygen present, creating a reduced environment rather than an oxidized one. The sample holder buffers the oxygen fugacity to the Ni-NiO buffer value. This would stabilize magnetite over hematite.

These reactions also produced a variety of minerals that fit relatively well on an AFM diagram (Figure 15), mapping the bulk composition of the sample and the relative proportion of the minerals. The dot in the Garnet-Biotite-Staurolite triangle represents the bulk composition while the location of the dot represents the relative proportions of these minerals. If this is the case, the reaction that took place was not exclusively between the garnet and the biotite. A different reaction might arise from a number of factors. The growth of spinel ($(Mg,Fe)Al_2O_4$) may result from using too little water included in the sample to keep the biotite stable. Though unlikely, water vapor may have leaked if the Au foil did not fully cover the samples in the porophyllite container. If the pressure fluctuated or dropped too much, water vapor may have been allowed to escape. The use of natural materials might also have had an impact on the

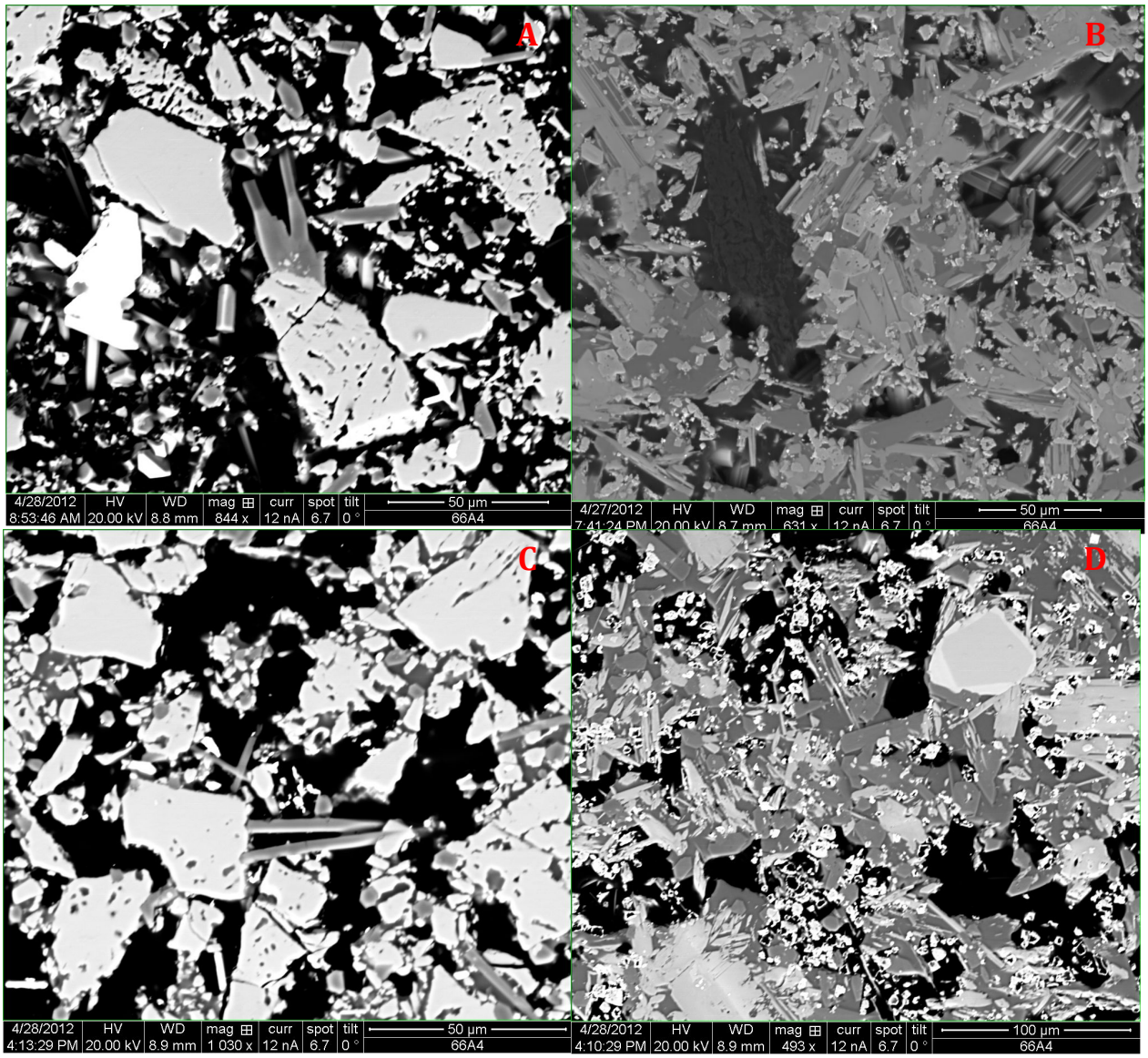

Figure 11: BEIs of each 700°C sample. A) Garnet and quartz. Alumino-silicate minerals growing from garnet into a blade-like shape. B) Kyanite and staurolite crystals C) Garnet and quartz crystals exhibiting a pitted texture with kyanite. D) Kyanite and staurolite crystals. Zoned garnet in the upper right corner.

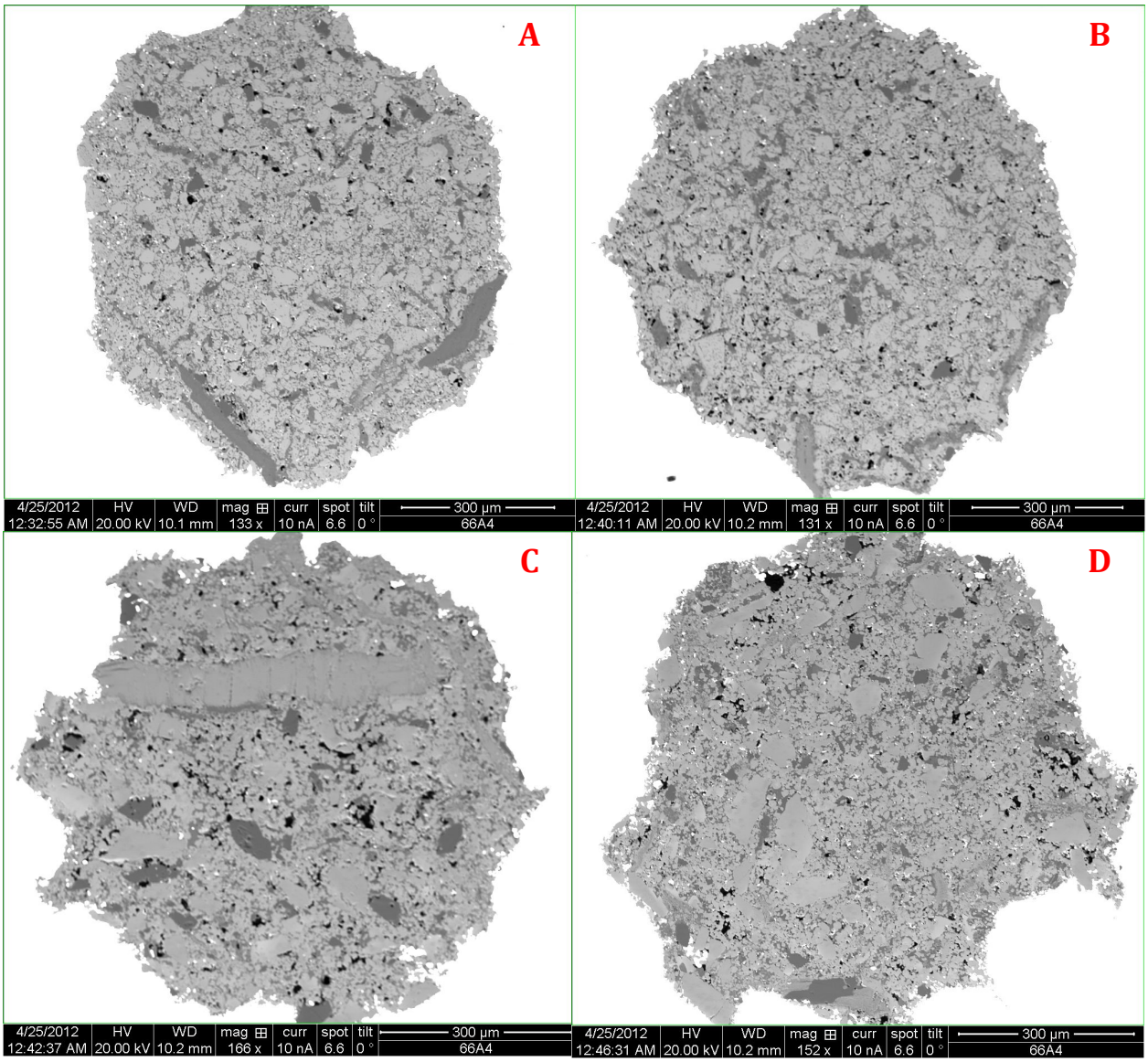

Figure 12: BEIs of each 800°C sample. A) Garnet and quartz with large alumino-silicate minerals B) Garnet, quartz and alumino-silicate minerals C) Biotitic melt, alumino-silicate minerals and garnet D) Garnet crystals, quartz and alumino-silicate minerals

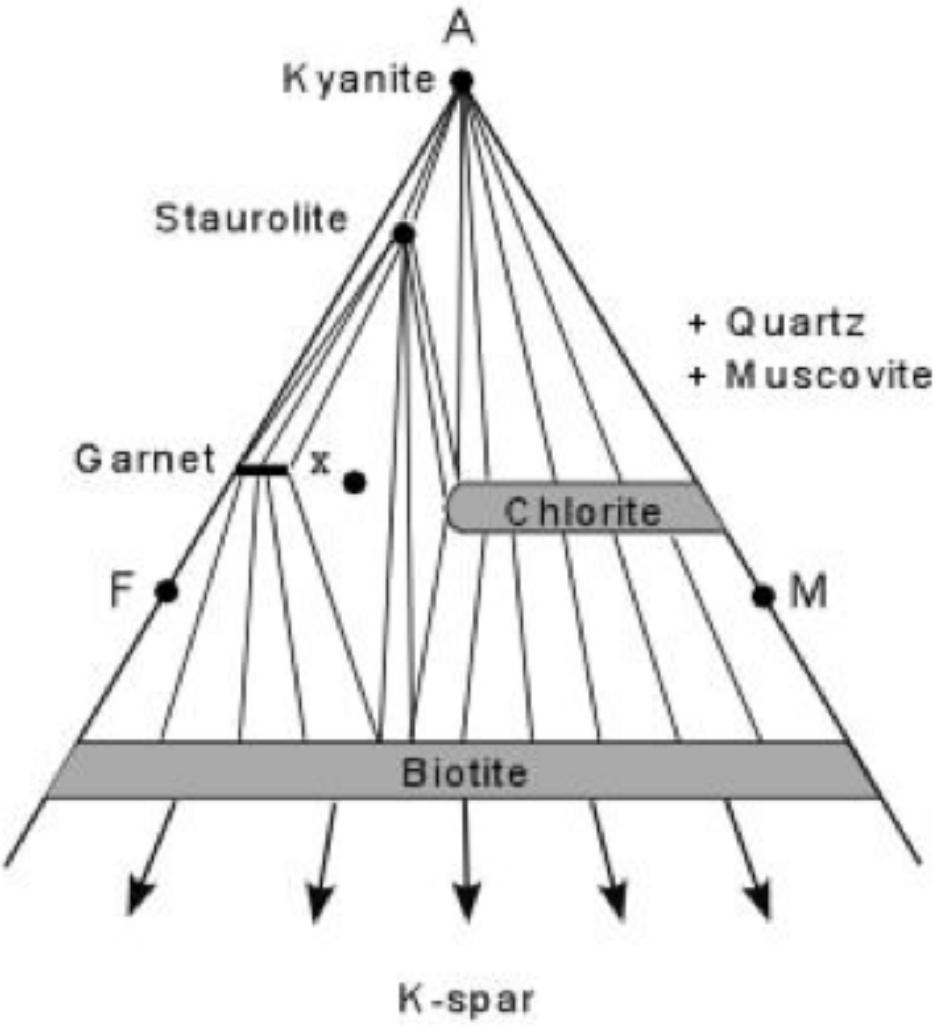

Figure 15: AFM diagram of the amphibolite facies. The amphibolie facies of medium pressures and average to high metamorphic temperatures. Tie lines are used to plot mineral relationships in metamorphic rocks based on bulk composition. Image credit geoscience forum, 2007.

chemical reactions taking place during the run. In addition, the garnets were shown to have inclusions that may have been exposed while powdering the garnet during the preparation. Staurolite ($Fe_2Al_9O_6(SiO_4)_4(OH)_2$ is the third mineral in the mineralogical relationship between

biotite and garnet ties under the amphibolite facies conditions as illustrated by the ties in Figure 15.

The BEI of Figure 6A shows the conchoidal fracture and absence of any visible crystals in the almandine glass produced by the second almandine homogenizing run. These two characteristics are the primary evidence that the second almandine homogenization run melted. Conchoidal fracture is characteristic of glass and minerals with weak or no cleavage. The composition of the garnet glass produced by this run (Appendix B, column 7) is unusual because it contains Na. Though Na is not present in the source-rock almandine, the presence of Na and Cl in the garnet glass indicates that NaCl from the halite sleeve contaminated the sample either during the homogenizing run or its preparation. This contamination most likely occurred because the salt was molten during the homogenization run and breached the pyrex sleeve that separated it from the garnet (Figure 1). This run also consistently experienced excess pressures through the course of its duration, exceeding 9kb at its maximum. However, high pressures tend to cancel the effects of high temperatures and do not generally facilitate melting, so it is likely that it was the NaCl contamination that led to the unexpected melting.

High magnesium content of garnet in pelitic rocks is typically associated with high temperatures, meaning that the high-magnesium garnets grew at higher temperatures. As the garnets were nucleating during the synthesis run, the high temperatures produced a higher concentration of Mg in the garnet crystals. This would explain the increase in the Mg/Fe ratio from the garnet glass to the synthesized garnet crystals, leaving a higher concentration of Fe in the glassy matrix of the synthesis run. After the homogenization run melted, we could not use the material, although the composition was homogenous, because there is too high a proportion of glass to crystals and the glass could react with and affect the biotite compositions.

The calculated formulas of the source and homogenized garnets in Appendix B do not fit the number of 2+ valence electrons in the chemical formula of garnet: $(Mg,Fe)_3Al_2(SiO_4)_3$. For example, the charges in the calculated formula, $Fe_{0.47}Mn_{0.22}Mg_{0.39}Ca_{0.08}Na_{0.17}Al_{1.45}(Si_{2.40}O_4)_3$, were calculated to be only add up to 1.33 atoms when three are required in the chemical formula. This happened because the chemical analysis was not calibrated against a standardized garnet formula, because no standard accounted for the Na detected by the SEM. If the weight percentage was not accurately calculated by normalizing the quantification, the results would be inaccurate. Therefore we were unable to calculate chemical formulas of the garnets analyzed because the added weight percentage of the samples was inaccurate. This accounts for all the source material garnet and homogenization runs compositional inadequacies.

Oxide Wt%	1.	2.	3.	4.
Na_2O	----------	----------	----------	----------
MgO	0.72	5.29	6.66	1.16
Al_2O_3	16.67	17.75	21.46	15.30
SiO_2	28.26	29.61	42.10	27.92
K_2O	----------	----------	----------	----------
CaO	4.78	0.87	0.74	3.56
TiO_2	----------	----------	----------	----------
MnO	6.53	0.43	----------	----------
FeO	21.18	25.40	22.45	23.87
Total	78.140	79.350	93.41	71.80
Si	1.959	1.957	2.222	2.084
Ti	----------	----------	----------	----------
Al	1.362	1.383	1.335	1.346
Fe	1.228	1.404	0.989	1.399
Mn	0.383	0.024	----------	----------
Mg	0.074	0.521	0.524	0.129
Ca	0.355	0.062	0.042	0.285
Na	----------	----------	----------	----------
K	----------	----------	----------	----------
Mg #	80	79	84	78

Table 4: Recalculated values of source almandine, source pyrope, homogenized almandine and homogenized pyrope, respectively.

Aside from the biotite observed in the 800°C run, no biotite was found in the experimental ion exchange runs. This is partly due to the very small ratio of biotite to garnet. However, the new chemical reactions are primarily driven by the loss of water in the system, accounting for biotite's scarcity in the experimental ion exchange samples.

CONCLUSIONS

Several types of mechanical malfunctions did occur during the course of this experiment. Hydraulic fluid leaks in the lower ram caused drops in pressure that caused the thermocouple assembly to lose contact with the sample. However, these changes in pressure did not visibly affect the chemical reactions taking place. The garnet analyses of the source materials and homogenization runs could not be calculated using standards because of the Na content in the samples. Therefore the analyses cannot produce an accurate analysis of the garnet formula. When the mineral formulas were recalculated after a second analysis excluding the Na peak, the weight percentages were much more accurate. As a result, the calculated garnet formula for the homogenized almandine was much more accurate than the normalized formulas calculated in Appendix B though still not wholly accurate.

The synthesis run was the only run that produced expected results. However, a longer period of time was needed to produce enough of a garnet:glass ratio for the material to have been any use in the experimental ion exchange runs. The garnet crystals were euhedral in shape with a resonable change in the Mg number tracking the changes in composition. The sample assembly was breached by molten NaCl, which contaminated the garnet and produced melting.

The chemical reactions in this experiment did not follow the expected reaction. First, the loss of biotite was due to a dehydration of the sample assembly during the course of the 600°C and 700 °C experimental ion exchange runs and a small ratio of biotite to garnet (2:98). The

800°C run was the only experimental run that retained any biotite to be analyzed by the SEM. However, the disappearance of K in the samples is unexplained. Even with a 50:1 garnet to biotite ratio not much new material will be created by the breakdown of biotite due to dehydration.

This lack of biotite does not allow for a geothermometer to be calculated from the data. In addition, the use of natural materials from garnet inclusions introduced other elements into the equation such as Na as observed in the almandine-rich garnet. Despite this challenge, the Mg-richer and Mg-poorer compositions of the biotite found in the 800°C run all have the same relative same composition (Appendix B). This means that the garnet-biotite thermometer chemical reactions happened as expected, the bulk compositions of be Mg-rich biotite and the Fe-rich biotite reached the equilibrium tie line as shown in Figure 4.

The presence of staurolite in the 600°C experimental ion exchange run is evidence that the bulk composition was not entirely garnet and biotite. Instead of producing a garnet-biotite geothermometer, this experiment has undergone entirely new reactions reflecting our simulated metamorphic conditions and resulting reactions of a pelitic amphibolite facies.

References

Chunming, Wu, Yusheng, Pan. Reviews in Garnet-Biotite Geothermometer: Its Versions, Inherent Problems of Accuracy and Precision and Perspective for Further Research. *Chinese Journal of Geochemistry*, Vol 18, No. 1. (1999) p. 54-61.

Dallmeyer, R. D., Mineralogical Notes: The Role of Crystal Structure in Controlling the Partitioning of Mg and Fe^{2+} Between Coexisting Garnet and Biotite. *American Mineralogist*, Vol 59 (1974) p. 201-203.

Dasgupta, Sommath, Pulak, Sengupta, Dipayan, Guha, Fukuoka, M., A refined garnet-biotite Fe-Mg exchange geothermometer and its application in amphibolites and granulites. *Contributions to Mineralogy and Petrology* Vol 109. (1991) p. 130-137

Ferry, J. M. and Spear, F. S., Experimental Calibration of the partitioning of Fe and Mg Between Biotite and Garnet. *Contributions to Mineralogy and Petrology* Vol 66 (1978) p. 113-117

Ganguly, J., Cheng, W. and Tirone, M. (1996)Thermodynamics of aluminosilicate garnet solid solution: new experimental data, an optimized model, and thermometric applications. *Contributions to Mineralogy and Petrology*, 126, p.137 –151.

Ghent, E.D. & Stout, M.Z. 1981: Geobarometry and geothermometry of plagioclase-biotite-garnet-muscovite assemblages. *Contributions to Mineralogy and Petrology 76*, 92-97.

Holdaway, MJ, Mukhopadhyay, Biswajit, Dyar, MD, Guidotti, CV, Dutrow, BL. Garnet-biotite geothermometery revised: New Margules parameters and a natural specimen data set from Maine. *American Mineralogist* Vol 82. (1997) p. 582-595

Kleeman,U. & Reinhart, J. 1994: Garnet-biotite thermometry revisited: the effect of AlVI and Ti in biotite. *European Journal of Mineralogy 6*, 925-941.

Lang, H.M. and Rice, J.M. (1985*b*) Geothermometry, geobarometry and *T-X*(Fe-Mg) relations in metapelites, Snow Peak, northern Idaho. *Journal of Petrology*, 26, 889 – 924.

McClellan, E.A., 1994a: Contact relationships in the southeastern Trondheim Nappe Complex, central-southern Norway: implications for early Paleozoic tectonism in the Scandinavian Caledonides. *Tectonophysics 231*, 85-111.

McClellan, E.A. 1994b: Textural zoning in garnet from the Einunnfjellet–Savalen area, south-central Norwegian Caledonides.*Geological Society of America Abstracts with Programs 26*, 56.

McClellan, E.A. 2004. Metamorphic conditions across the Seve-Köli Nappe boundary, southeastern Trondheim region, Norwegian Caledonides: Comparison of garnet-biotite thermometry and amphibole chemistry. *Norweigian Journal of Geology*. Vol 84 No 4.

Mukhopadhyay, B., Holdaway, M.J. and Koziol, A.M. (1997) A statistical model of thermodynamic mixing properti es of Ca-Mg-Fe2+ garnets. *American Mineralogist*, 82, p. 165 –181.

Nesse, William D. 2000: *Introduction to Mineralogy*, 1st edition. Oxford University Press, New York, p 246-248, 310-312, 362-363.

Osberg, Philip H. An equilibrium model for Buchan-type metamorphic rocks, South-Central Maine. *American Mineralogist*, Vol 56 (1971) p. 570-586.

Perchuk LL, Lavrenteva IV (1983) Experimental investigation of exchange equilibria in the system cordierite - garnet - biotite. Saxena SK (ed) Kinetics and equilibrium in mineral reactions. Springer Berlin, Heidelberg, New York, pp. 199 239

Lavrent'eva, I.V., Perchuk, L.L., 1981. Phase correspondence in the system biotite– garnet: experimental data. Dokl. Akad. Nauk SSSR 260, 731– 734.

Spear, F.S. 1993: *Metamorphic phase equilibria and pressuretemperature- time paths*. Mineralogical Society of America, Washington, D.C., 799 pp.
Turner, F.J. 1981: *Metamorphic petrology*, 2nd edition. McGraw-Hill, New York, 524 pp.

Appendix A

Pyrope Homogenizing Run

Date	Time	Temperature	Output Power	Upper Ram	Lower Ram	Increase/ Decrease
2/4/12	10:53	20	0	6800	2550	
	10:53	100	11.7	6800	2550	
	10:54	200	17.9	6800	2550	
	10:55	300	22.5	6800	2550	
	10:56	400	26.3	6800	2550	
	10:57	500	30.2	6800	2600	
	10:58	600	34.9	6800	2600	
	10:59	700	39.8	6800	2400	
	11:00	800	44.5	6800	2500	
	11:08	1300	70.2	7180	2600	
	14:06	1300	72.3	7750	2750	
	15:34	1300	71.7	7800	2700	
	18:19	1300	70.4	7800	2610	
	21:02	1300	69.1	7800	2600	
	22:32	1300	67.3	7750	2490	Lower Ram-2700
2/5/12	9:20	No Reading	No Reading	No Reading	No Reading	

* There was a hydraulic fluid leak in the piston cylinder press that caused a pressure failure so that the thermocouple assembly did not complete its electrical circuit. Therefore, there was no reading when next checked at 9:20 on 2/5/12.

Almandine Homogenizing Run

Date	Time	Temperature	Output Power	Upper Ram	Lower Ram	Increase/ Decrease
2/5/12	17:37	20	0.0	6500	2550	
	17:38	100	13.4	6500	2550	
	17:39	200	19.5	6450	2550	
	17:40	300	24.0	6450	2550	
	17:41	400	27.4	6500	2500	
	17:42	500	31.2	6500	2500	
	17:43	600	36.0	6500	2450	Lower Ram-2600
	17:44	700	41.3	6550	2500	Lower Ram-2650
	17:45	800	46.7	6600	2600	
	17:46	900	51.3	6600	2450	Lower

						Ram-2600
	17:47	1000	56.8	6600	2600	
	17:48	1100	62.5	6650	2600	
	17:49	1200	66.4	6700	2600	
	17:52	1300	70.9	6800	2610	
	19:54	1300	73.0	7300	2800	Lower Ram-2750
	22:12	1300	72.8	7400	2800	Lower Ram-2610
	23:00	1300	72.6	7400	2650	
2/6/12	5:15	1300	70.8	7380	2630	Lower Ram-2800
LIGHT	7:09	1300	54.3	7380	2400	Lower Ram-2650
	8:35	1300	48.7	7100	2000	
	9:00	1300	49.1	7100	2520	
	10:40	1300	49.3	7100	2500	
	10:53	1300	49.5	7100	2560	
	12:37	1300	49.9	7100	2610	
	13:00	1300	49.9	7100	2550	
	15:05	1300	50.3	7100	2400	
	17:15	1300	50.6	7100	2600	
	19:27	1300	51.0	7100	2600	
	20:37	1300	51.0	7100	2600	
	22:43	1300	51.3	7100	2600	
2/7/12	0:00	1300	51.4	7100	2600	
	7:11	1300	51.7	7150	2610	
	8:20	1300	51.9	7130	2610	
	10:17	1300	52.1	7150	2590	
	11:53	1300	52.1	7130	2510	
	12:56	1300	52.2	7160	2490	Lower Ram-2650
	15:12	1300	48.7	7100	2400	Lower Ram-2650
	17:07	1300	48.7	7080	2550	Lower Ram-2650
	19:39	1300	48.2	7090	2780	Lower Ram-2650
	20:08	1300	48.1	7090	2750	Lower Ram-2850

LIGHT means that the alarm light was lit at the time checked. The alarm light goes off if temperature fluctuated by greater than 5°C.

Melted Almandine Homogenizing Run

Date	Time	Temperature	Output Power	Upper Ram	Lower Ram	Increase/ Decrease
2/15/12	17:25	19	0.0	6500	2550	
	17:26	100	15.9	6500	2550	
	17:27	200	25.5	6500	2550	
	17:28	300	31.9	6550	2600	
	17:29	400	37.6	6550	2600	
	17:30	500	41.6	6550	2500	Lower Ram-2600
	17:31	600	46.7	6550	2600	
	17:32	700	52.2	6650	2600	
	17:33	800	55.7	6650	2600	
	17:34	900	63.4	6720	2600	
	17:35	1000	68.8	6770	2600	
	17:36	1100	75.2	6770	2600	
	17:37	1200	81.0	6880	2720	
	17:39	1300	85.2	6980	2800	Lower Ram-2680
	17:59	1300	85.2	7360	2850	Lower Ram-2650
	16:11	1300	84.8	7470	2760	
LIGHT	18:46	1300*	86.5	7650	2900	Lower Ram-2650
LIGHT	20:59	1300*	83.4	7750	2750	Lower Ram-2650
	23:04	1300*	82.5	7750	2690	
2/16/12	6:11	1300*	79.4	7750	2490	Lower Ram-2650
	8:19	1300*	79.5	7775	2650	
	10:30	1300	79.2	7775	2650	
	11:51	1300	79.2	7800	2690	
	14:00	1300*	79.4	7800	2610	
	16:08	1300*	79.3	7800	2610	
	17:11	1300	79.4	7770	2620	
	19:47	1300*	79.2	7770	2610	
	20:50	1300	79.3	7780	2630	
	21:40	1300	79.0	7780	2630	
	22:51	1300*	79.3	7800	2650	
2/17/12 LIGHT	7:25	1300*	82.9	7900	2830	Upper Ram-7500 Lower Ram-2610
	10:00	1300*	82.5	7490	2690	

	13:08	1300*	83.4	7490	2690	
	15:03	1300	83.3	7490	2690	
	19:23	1300*	82.3	7490	2680	
	22:07	1300*	81.6	7420	2650	
	23:06	1300	80.8	7420	2650	
2/18/12	7:27	1300*	79.9	7420	2610	
	11:21	1300	78.5	7400	2520	Lower Ram-2620
	14:22	1300	77.7	7350	2510	Lower Ram-2620
LIGHT	16:02	1300	77.1	7310	2590	
	18:44	1300	77.1	7310	2550	Lower Ram-2650
LIGHT	22:26	1300*	76.8	7350	2690	
2/19/12 LIGHT	7:23	1300*	86.2	7620	3300	

Failed Synthesis Run

Date	Time	Temperature	Output Power	Upper Ram	Lower Ram	Increase/ Decrease
2/25/12	11:46	20	0.0	6820	4600	
	11:47	100	20.0	6820	4600	Lower Ram-4890
	11:48	200	28.4	6890	4850	
	11:49	300	34.8	6890	4810	
	11:50	400	39.0	6890	4720	Lower Ram-4890
	11:51	500	41.6	6920	4800	
	11:52	600	44.8	6950	4750	Lower Ram-4890
	11:53	700	48.6	7000	4800	
	11:54	800	53.0	7020	4760	Lower Ram-4890
	11:55	900	56.2	7090	4850	
	11:56	1000	56.9	7110	4890	

	11:59	1100	59.3	7210	4910	
	13:36	1100	65.0	7810	4920	
LIGHT	14:26	1098	67.5	7850	4920	
LIGHT	15:19	1099	70.3	7910	4950	

Synthesis Run

Date	Time	Temperature	Output Power	Upper Ram	Lower Ram	Increase/ Decrease
2/25/12	20:55	20	0.0	6750	4650	
	20:56	100	17.4	6790	4900	
	20:57	200	27.8	6790	4850	
	20:58	300	33.5	6790	4800	Lower Ram-4890
	20:59	400	38.2	6820	4800	
	21:00	500	41.3	6850	4700	Lower Ram-4900
	21:01	600	43.9	6890	4710	
	21:02	700	46.6	6910	4750	Lower Ram-4800
	21:03	800	50.7	6950	4810	
	21:04	900	55.8	6990	4700	Lower Ram-4900
	21:05	1000	59.9	7010	4810	Lower Ram-4900
	21:08	1100	65.2	7110	4900	
	22:26	1100	64.4	7730	5100	
2/26/12	7:22	1100	60.7	7800	4990	
	10:31	1100	61.1	7800	4950	
	11:36	1100	61.3	7810	4950	
	15:03	1100	61.4	7810	4910	
	18:29	1100	61.0	7810	4910	
	20:56	1100	61.2	7810	4910	
	21:50	1100	61.3	7810	4910	

600°C Experiment

Date	Time	Temperature	Output Power	Upper Ram	Lower Ram	Increase/ Decrease
3/16/12	16:06	21	0.0	6550	2610	
	16:07	100	17.6	6590	2610	
	16:08	200	26.1	6600	2710	

	16:09	300	32.4	6610	2810	
	16:10	400	37.7	6690	2910	
	16:11	500	41.1	6700	3000	Lower Ram- 2600
	16:14	600	44.4	6750	2690	
	16:54	600	44.5	7210	2910	
	23:30	600	44.7	7510	2900	
3/17/12	6:13	600	44.7	7510	2910	
	15:48	600	44.8	7400	2850	
	17:00	600	44.7	7430	2850	Lower Ram- 2750
3/18/12	11:35	600	44.4	7370	2710	
3/19/12	9:15	600	44.9	7380	2710	
	11:05	600	44.8	7380	2710	
	12:10	600	44.9	7380	2710	
	14:19	600	44.7	7400	2710	
3/20/12	9:15	600	45.1	7430	2710	
	11:54	600	45.0	7430	2710	
	13:55	600	44.9	7410	2710	
3/21/12	9:14	600	44.9	7400	2700	
	10:14	600	44.8	7400	2700	
	13:19	600	45.1	7420	2700	
	14:15	600	44.8	7450	2710	
3/22/12	9:13	600	45.0	7410	2700	
	12:40	600	45.4	7410	2700	
	14:13	600	45.0	7410	2710	
3/23/12	9:25	600	45.2	7410	2690	
	14:13	600	45.1	7400	2700	
	20:03	600	44.4	7400	2700	
3/24/12	7:35	600	45.0	7400	2690	
	12:05	600	45.1	7400	2690	
	15:36	600	45.2	7400	2670	
	20:36	600	44.6	7400	2650	
3/25/12	8:11	600	45.5	7400	2670	
	9:44	600	45.3	7400	2690	
	13:32	600	45.0	7400	2670	
	17:01	600	45.1	7420	2670	
3/26/12	8:40	600	45.3	7410	2650	
	9:03	600	45.3	7410	2670	
	12:39	600	45.3	7410	2670	

	18:38	600	45.3	7410	2690	
3/27/12	5:20	600	44.6	7410	2690	
	8:20	600	44.8	7410	2660	
	15:01	600	45.0	7410	2650	
	17:35	600	45.0	7410	2650	
3/28/12	8:53	600	45.0	7410	2650	
	18:56	600	45.4	7430	2670	
	19:22	600	45.1	7410	2690	
	22:40	600	44.6	7410	2670	
3/29/12	11:55	600	44.8	7410	2610	
	18:37	600	45.1	7400	2610	
	20:49	600	44.6	7390	2610	
3/30/12	12:08	600	45.7	7400	2610	
3/31/12	13:30	600	45.7	7400	2610	
	14:25	600	45.7	7400	2610	
4/1/12	6:35	600	45.2	7390	2610	
	9:53	600	45.3	7390	2600	
	16:57	600	45.1	7370	2600	
	20:26	600	44.8	7390	2610	
4/2/12	9:50	600	45.2	7350	2590	
	13:20	600	45.2	7350	2600	
	20:27	600	44.6	7390	2610	

700°C Experiment

Date	**Time**	**Temperature**	**Output Power**	**Upper Ram**	**Lower Ram**	**Increase/ Decrease**
4/4/12	21:03	21	0.0	6490	2490	Lower Ram-2690
	21:04	100	21.8	6500	2610	
	21:05	200	30.1	6500	2610	
	21:06	300	35.6	6510	2550	
	21:07	400	40.1	6550	2510	Lower Ram-2650
	21:08	500	43.7	6590	2590	
	21:09	600	46.2	6600	2510	Lower Ram-2650
	21:12	700	49.6	6690	2490	Lower Ram-2690
4/5/12	9:00	700	49.3	7300	2500	Lower Ram-2650
	10:27	700	49.3	7300	2610	

	11:56	700	49.9	7300	2600	Lower Ram-2650
	16:18	700	50.1	7300	2610	
	19:30	700	50.1	7300	2600	
	22:01	700	49.1	7300	2590	Lower Ram-2650
4/6/12	8:30	700	49.9	7280	2590	Lower Ram-2650
	9:20	700	49.9	7290	2610	
	10:58	700	49.7	7290	2610	
	16:20	700	49.8	7280	2600	
	19:27	700	49.9	7250	2600	Lower Ram-2690
4/7/12	8:33	700	49.5	7280	2610	
	16:33	700	49.4	7280	2610	
	19:41	700	49.3	7280	2610	
4/8/12	12:44	700	49.6	7230	2590	Lower Ram-2690
	19:09	700	49.6	7250	2610	
4/9/12	9:58	700	49.7	7250	2610	
	20:20	700	48.9	7250	2610	
4/10/12	15:05	700	49.2	7210	2590	Lower Ram-2690
4/11/12	10:03	700	49.3	7210	2610	
4/12/12	11:52	700	49.3	7250	2650	
	18:46	700	49.6	7250	2610	
4/13/12	10:55	700	49.2	7210	2590	Lower Ram-2650
4/14/12	16:40	700	49.2	7210	2610	
	19:05	700	49.3	7210	2610	

800°C Experiment

Date	**Time**	**Temperature**	**Output Power**	**Upper Ram**	**Lower Ram**	**Increase/ Decrease**
3/1/12	16:13	20	0.0	6510	2400	
	16:14	100	22.8	6510	2400	Lower Ram-2610
	16:15	200	30.3	6520	2610	
	16:16	300	35.5	6550	2520	Lower Ram-2650

	16:17	400	39.9	6590	2590	
	16:18	500	43.0	6610	2490	Lower Ram-2610
	16:19	600	46.5	6620	2500	
	16:20	700	49.2	6650	2390	Lower Ram-2610
	16:23	800	53.7	6790	2600	
	17:43	800	52.6	7320	2650	
	20:03	800	52.5	7410	2690	
	22:36	800	52.3	7410	2690	
3/2/12	10:00	800	52.8	7450	2610	
	10:55	800	53.1	7490	2610	
	14:35	800	53.2	7490	2600	
	15:16	800	53.2	7490	2610	
	18:05	800	53.1	7490	2600	
3/3/12	5:37	800	53.0	7490	2590	Lower Ram-2610
	9:46	800	53.2	7490	2600	
	13:07	800	53.2	7450	2590	Lower Ram-2630
	18:02	800	53.0	7450	2590	Lower Ram-2650
	21:30	800	53.2	7490	2610	
3/4/12	8:52	800	53.2	7490	2610	
	19:44	800	53.0	7410	2550	Lower Ram-2650
3/5/12	8:17	800	53.5	7490	2700	
	9:00	800	53.5	7490	2700	
	10:51	800	53.5	7490	2700	
	13:12	800	53.5	7490	2700	
	17:01	800	53.6	7490	2690	
	20:51	800	53.2	7490	2690	
3/6/12	8:34	800	53.4	7450	2680	
	17:50	800	53.1	7420	2610	
	20:39	800	45.0	7290	2290	Lower Ram-2650

	21:59	800	44.1	7190	2450	Lower Ram- 2690
3/7/12	5:38	800	43.9	7150	2590	Lower Ram- 2690
	7:52	800	44.0	7150	2650	
	10:48	800	44.3	7110	2610	
	14:30	800	44.3	7130	2600	
	15:53	800	44.4	7120	2600	
	17:00	800	44.2	7150	2600	
3/8/12	7:17	800	44.0	7110	2610	
	10:12	800	44.5	7120	2610	
	11:52	800	44.4	7120	2610	
	15:17	800	44.6	7120	2610	
	18:30	800	44.5	7180	2650	
	19:51	800	44.6	7190	2650	
3/9/10	7:43	800	45.3	7190	2650	
	10:00	800	45.8	7190	2690	
	13:51	800	46.0	7200	2690	
	18:07	800	46.8	7220	2710	
	19:27	800	47.2	7290	2750	
3/10/12	6:07	800	49.3	7410	2890	
	11:01	800	50.4	7410	2900	
	11:57	800	50.6	7430	2900	
	15:16	800	50.6	7410	2900	
	19:07	800	50.9	7410	2910	
3/11/12	10:18	800	52.4	7500	3000	
	13:17	800	52.8	7500	2990	
	21:32	800	53.1	7510	3000	
3/12/12	8:13	800	54.3	7520	3050	

Appendix B: SEM compositional analyses

Oxide Wt%	1.	2.	3.	4.	5.	6.	7.	8.	9.
Na_2O	----------	---------	0.08	--------	1.03	1.92	5.81	3.76	1.32
MgO	12.49	6.94	1.53	10.05	1.94	5.63	4.54	3.18	6.32
Al_2O_3	15.92	20.81	29.57	29.33	28.59	26.56	26.94	25.14	27.78
SiO_2	33.91	38.46	59.08	55.1	59.2	51.77	57.17	64.14	59.84
K_2O	8.8	10.22	---------	--------	--------	---------	--------	-------	-------
CaO	----------	---------	2.89	0.43	2.88	1.53	1.49	1.59	1.13
TiO_2	2.23	2.14	---------	--------	--------	---------	--------	-------	-------
MnO	----------	---------	2.54	0.16	1.22	0.56	0.81	0.34	0.83
FeO	11.98	20.05	4.31	4.93	5.14	12.03	3.24	1.86	2.79
Total	85.33	98.62	100.00	100.00	100.00	100.00	100.00	100.01	100.01
Si	3.047	3.065	2.602	2.425	2.613	2.395	2.605	2.779	2.605
Ti	0.151	0.128	---------	--------	--------	---------	--------	-------	-------
Al	1.686	1.955	1.535	1.522	1.487	1.448	1.426	1.284	1.426
Fe	0.900	1.336	0.159	0.181	0.190	0.465	0.102	0.067	0.102
Mn	----------	---------	0.095	0.006	0.046	0.222	0.031	0.012	0.031
Mg	1.673	0.824	0.100	0.659	0.128	0.388	0.410	0.205	0.410
Ca	----------	---------	0.136	0.020	0.136	0.076	0.053	0.074	0.053
Na	----------	---------	0.007	--------	0.088	0.172	0.111	0.316	0.111
K	1.009	1.039	---------	--------	--------	---------	---------	-------	-------
Mg #	89	85	97	96	96	91	97	99	98

1. Phlogopite
2. Annite
3. Source almandine
4. Source pyrope
5. Homogenized almandine
6. Homogenized pyrope
7. Melted glass from second almandine homogenizing run
8. Glass from synthesis run
9. Garnet from synthesis run

Oxide Wt%	10.	11.	12.	13.	14.	15.	16.	17.
Na_2O	---------	--------	1.17	---------	---------	---------	---------	--------
MgO	4.40	6.82	9.02	11.02	1.24	1.32	---------	1.04
Al_2O_3	12.74	71.88	20.26	79.94	16.61	17.69	30.68	17.53
SiO_2	39.47	11.01	59.99	---------	27.79	29.03	54.89	29.01
K_2O	---------	--------	--------	---------	---------	---------	---------	--------
CaO	2.31	--------	0.60	---------	3.08	3.16	9.66	3.35
TiO_2	---------	--------	--------	---------	0.54	---------	---------	0.48

MnO	1.22	--------	--------	---------	2.99	2.97	0.59	2.96
FeO	26.59	10.29	8.96	9.04	22.30	23.29	4.18	23.07
Total	86.730	100.000	100.000	100.000	74.550	77.460	100.000	77.440
Si	2.361	0.262	2.688	---------	1.983	1.990	1.231	1.989
Ti	---------	--------	--------	---------	0.029	---------	---------	0.025
Al	0.898	2.019	1.070	2.280	1.397	1.429	0.811	1.417
Fe	1.330	0.205	0.336	0.183	1.331	1.335	0.078	1.323
Mn	0.062	---------	--------	---------	0.181	0.172	0.11	0.172
Mg	0.392	0.242	0.603	0.397	0.132	0.135	---------	0.106
Ca	0.148	---------	0.029	---------	0.236	0.232	0.232	0.246
Na	---------	---------	0.102	---------	---------	---------	---------	--------
K	---------	---------	--------	---------	---------	---------	---------	--------
Mg#	79	93	84	94	79	79	96	79

10. Garnet in 600°C experimental ion exchange Sample A (Figure 9A)
11. Spinel in 600°C experimental ion exchange Sample A (Figure 9A)
12. Garnet in 600°C experimental ion exchange Sample B (Figure 9B)
13. Spinel in 600°C experimental ion exchange Sample B (Figure 9B)
14. Garnet in 600°C experimental ion exchange Sample C (Figure 9C)
15. Garnet in 600°C experimental ion exchange Sample C (Figure 9C)
16. Unknown mineral in 600°C experimental ion exchange Sample C (Figure 9C)
17. Garnet in 600°C experimental ion exchange Sample D (Figure 9D)
18. Garnet in 600°C experimental ion exchange Sample D (Figure 9D)

Oxide Wt%	19.	20.	21.	22.	23.	24.	25.	26.
Na_2O	---------	--------	--------	---------	---------	---------	---------	--------
MgO	1.03	5.71	6.92	1.32	4.13	7.45	10.58	10.43
Al_2O_3	15.25	11.77	9.29	15.08	15.81	20.49	17.45	13.4
SiO_2	24.03	26.88	28.07	25.02	25.61	38.73	37.88	40.36
K_2O	---------	--------	--------	---------	---------	9.61	---------	--------
CaO	2.51	0.60	0.40	2.78	1.04	---------	---------	--------
TiO_2	0.39	--------	--------	0.72	---------	2.02	---------	--------
MnO	2.69	--------	--------	3.04	---------	---------	---------	--------
FeO	22.87	16.41	18	22.4	23.39	18.82	25.64	26.62
Total	67.770	61.370	62.680	70.360	69.980	97.120	91.550	89.830
Si	1.915	2.207	2.283	1.924	1.933	3.105	2.107	2.283
Ti	0.023	--------	--------	0.042	---------	0.122	---------	--------
Al	1.432	1.139	0.891	1.367	1406	1.936	1.144	0.894
Fe	1457	1.127	1.224	1.441	1.476	1.262	1.193	1.213
Mn	0.182	---------	--------	0.198	---------	--------	---------	--------
Mg	0.122	0.699	0.839	0.151	0.465	0.890	0.877	0.880
Ca	0.214	0.053	0.035	0.229	0.084	---------	---------	--------

Na	---	---	---	---	---	---	---	---
K	---	---	---	---	---	0.983	---	---
Mg#	78	82	81	78	78	85	82	79

19. Garnet in 700°C experimental ion exchange Sample A (Figure 10A)
20. Garnet in 700°C experimental ion exchange Sample B (Figure 10B)
21. Garnet in 700°C experimental ion exchange Sample B (Figure 10B)
22. Garnet in 700°C experimental ion exchange Sample C (Figure 10C)
23. Garnet in 700°C experimental ion exchange Sample D (Figure 10D)
24. Biotite in 800°C experimental ion exchange Sample A (Figure 11A)
25. Garnet in 800°C experimental ion exchange Sample A (Figure 11A)
26. Garnet in 800°C experimental ion exchange Sample A (Figure 11A)

Oxide Wt%	27.	28.	29.	30.	31.	32.	33.
Na_2O	---	---	---	1.58	---	---	---
MgO	16.46	9.98	1.47	0.96	9.03	15.02	14.94
Al_2O_3	18.92	21.6	19.6	38.31	27.91	19.61	19.42
SiO_2	43.56	34.38	33.67	55.13	59.27	40.49	39.79
K_2O	4.84	---	---	4.01	0.37	7.55	9.03
CaO	---	---	4.25	---	1.4	---	---
TiO_2	1.38	---	---	---	0.65	1.74	2
MnO	---	---	6.62	---	---	---	---
FeO	13.48	26.6	27.39		1.36	12.43	11.846
Total	98.640	92.560	93.000	99.990	99.990	96.840	97.070
Si	3.236	1.909	1.963	3.605	2.560	3.117	3.083
Ti	0.077	---	---	---	0.021	0.101	0.117
Al	1.656	1.414	1.346	2.953	1.421	1.779	1.773
Fe	0.837	1.235	1.335	---	0.049	0.800	0.770
Mn	---	---	0.327	---	---	---	---
Mg	1.823	0.826	0.128	0.94	0.581	1.724	1.725
Ca	---	---	0.265	---	0.065	---	---
Na	---	---	---	0.2	---	---	---
K	0.459	---	---	0.335	0.020	0.742	0.892
Mg#	90	81	79	100	99	90	91

27. Biotite in 800°C experimental ion exchange Sample B (Figure 11B)
28. Garnet in 800°C experimental ion exchange Sample B (Figure 11B)
29. Garnet in 800°C experimental ion exchange Sample C (Figure 11C)
30. Biotitic melt in 800°C experimental ion exchange Sample C (Figure 11C)
31. Garnet in 800°C experimental ion exchange Sample D (Figure 11D)
32. Biotite in 800°C experimental ion exchange Sample D (Figure 11D)
33. Biotite in 800°C experimental ion exchange Sample D (Figure 11D)